

EFFECT OF TENSION SOFTENING OF CONCRETE ON THE TENSION STIFFENING OF REBARS IN PLAIN AND FIBROUS CONCRETE

K. Noghabai, T. Olofsson
Luleå University of Technology, Division of Structural Engineering
Sweden

Abstract

Tension stiffening effect on rebars embedded in concrete prisms are investigated through computational as well as analytical methods and compared with experimental results. Both metallic (steel) and non-metallic (polyolefin and carbon) fibres of different dimensions are used in high-strength concrete. The softening behaviour of concrete determined by a uniaxial tensile procedure, was used in FEM and analytical models. The tension stiffening effect may be more dependent on the tensile behaviour of the concrete than on a relative slip between rebar and concrete.

Key words: Tension stiffening, Steel fibres, Non-metallic fibres, High-strength concrete, Uniaxial tensile test.

1 Introduction

The composite action of a tensioned rebar embedded in concrete is manifested in the so-called tension stiffening effect. Phenomenologically, the stiffness of the rebar is increased by the surrounding concrete as a conse-

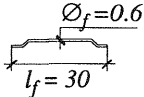
quence of the bond action between the two materials. An addition of fibres may help improving the bond and thus the function of a deformed reinforcement. Both types of reinforcements share also the mechanisms by which they interact with the surrounding material. Hence, the fibre-matrix interaction involve the local bonding capacity between a single fibre and the matrix, as fibres are meant to function after rupture of the concrete matrix. Earlier results have been presented in Noghabai (1997a, b, c).

2 Material and material properties

2.1 Concrete composition and types of fibres

The constituents of the HSC (dry material) in kg/m^3 were the following: 1152 coarse aggregates (12-16 mm), 730 sand (0-8 mm), 490 cement, 48 Silica fume and 4.62 superplasticizer mixed with 166 kg water per cubic metre concrete. The types of fibres are summarized in Table 1. Based on the cost and feasibility aspects, it is reasonable to keep the volume fraction of the fibres to approximately 1%. For the sake of convenience the batches and the elements are denoted by HSC indexed by the notations given in Table 1. The plain concrete is denoted HSC_{REF}. In the batch labelled HSC-Smix, the two types of steel fibres were combined to an equal amount (40 kg/m^3 of each type of fibre).

Table 1: Fibres used in the investigation

Notation	Material Type	Configuration	Aspect ratio, l_f / \varnothing_f	Density kg/m^3	Strength MPa	Elastic modulus GPa
S30/0.6	Steel Dramix®		50	7800	1100	200
S6/0.15	Steel Dramix®	—	40	7800	2600	200
P50/0.63	Polyolefin 3M™	—	79.4	910	275	2.6
P25/0.38	Polyolefin 3M™	—	65.8	910	275	2.6
Carbon	Carbon Dialead	—	($\approx 10^6$)	1600	4350	230

2.2 Behaviour of fibrous HSC in uniaxial tension

The tension softening behaviour of concrete reflects its resistance against crack extension. This behaviour makes a redistribution of stresses within a structure possible. The best way to obtain the relevant material properties (both in elastic and post-failure stage) is by a direct, uniaxial tensile test conducted in displacement control. For this reason test pieces were prepared from 74 mm cylindrical cores. Notched specimens of length 85 mm were produced from the cores, according to the inlaid picture in Fig. 1. The testing procedure has been described in Groth and Noghabai (1996). Fig. 1 shows the mean or typical post-tensile strength stresses, σ_f , versus the crack opening displacements (COD), w , curves. (That is when the elastic unloading of the bulk outside the localized crack plane is subtracted.) The area under the σ_f - w curve may represent the amount of energy (G_f) required to separate the notched specimen. It is evident from Fig. 1 that for capacity assessment of structures of fibrous concrete, the total amount of G_f cannot be relevant as it involves CODs of several millimetres. On the other hand for structures of plain concrete the CODs associated with consumption of the total G_f is possible and thence G_f might be used explicitly as a material parameter. In a more general sense, the shape of the curves and the amount of energy released up to the pertinent CODs are more relevant. The material properties of the concretes are tabulated in Table 2.

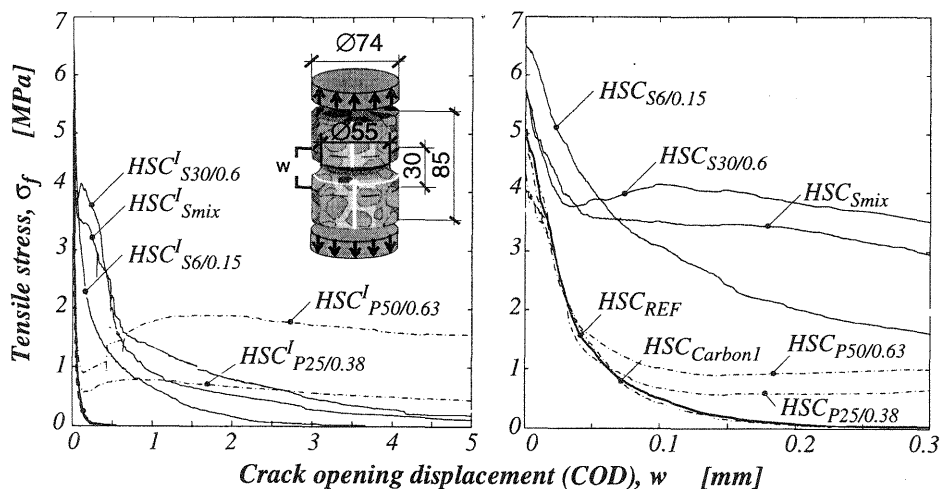


Fig. 1. The responses of different concretes to uniaxial tension.

Table 2: Material properties of concrete.

Denomination of the beams	Modulus of elasticity, E_c GPa	Compressive strength, f_{cc} * MPa	Tensile strength, f_{ct} MPa	Fracture energy, G_f N/m
HSC _{REF}	41.5 (2.4 [†])	121.6 (3.5)	5.01 (0.71)	216 (61)
HSC _{S30/0.6}	36.7 (0.9)	129.6 (2.3)	5.68 (0.26)	4044 (75)
HSC _{S6/0.15}	38.4 (4.4)	132.3 (2.8)	6.04 (0.67)	2025
HSC _{Smix}	36.5	127.0 (2.4)	5.75	5116
HSC _{P50/0.63}	39.2	129.0 (3.9)	5.16	2114
HSC _{P25/0.38}	32.5 (3.8)	117.5 (3.0)	4.39 (0.70)	4889 (777)
HSC _{Carbon1}	30.6 (5.6)	90.0 (1.8)	4.46 (0.38)	198 (23)
HSC _{Carbon2}	30.0 (2.0)	85.0 (2.1)	4.21 (0.41)	151 (12)

*. Tests on 100 mm cubes.

†. Standard deviation given for mean values. If absent the given value is based on a single test.

3 Experiments

3.1 Specimens and experimental set-up

The RILEM Technical Committee FMB-147 announced a Round-Robin Test and Analysis on Bond with specifications on the dimensions and production of the test pieces as well as the experimental set-up and procedures, see RILEM TC 147-FMB (1996). The experiments herein follow these recommendations as far as the dimensions, curing conditions of the specimens and experimental set-up concern.

A deformed $\varnothing 16$ mm bar of the Swedish grade Ks500 (nominal yield strength 500 MPa) is placed centric in a concrete prism. The prism has a square cross-section and measures $80 \times 80 \times 960$ mm² (i.e. the concrete cover is $2 \times \varnothing$, the prism length is $60 \times \varnothing$ and the reinforcement ratio is 0.031), see Fig. 2. The rebar has a asymmetric configuration of the lugs. The specimens were cast horizontally and cured in water for seven days. Then they were stored in approximately 60% relative humidity at about 20°C and kept in this condition up to one week before testing.

Only one tie element was produced from each batch. The elements were tested in a servohydraulic testing machine with a capacity of 60 tons.

The experiments were performed in displacement control. The distance between the grips was 990 mm. The displacement of the specimen was monitored by 4 linear voltage differential transducers (LVDT), see Fig. 2. During the testing, the crack widths were measured along the element by a magnifier (8 times). The crack width measurement was carried out on two opposed faces of the specimen generally at load intervals of 10 kN up to the occurrence of steel yielding and on a more random basis beyond the yielding point of the steel.

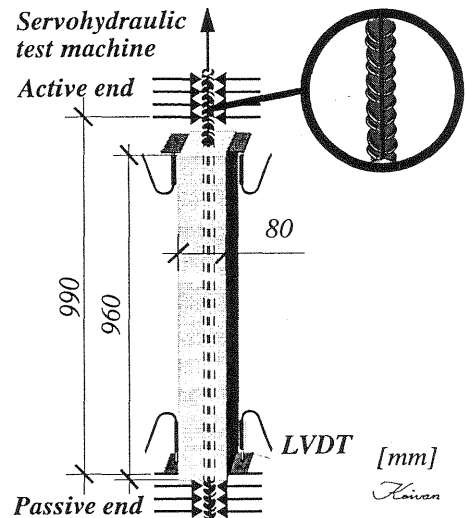


Fig. 2. The set-up of the pull-tension test.

3.2 Experimental observations and results

The results of the tests are given in Fig. 3. The major cracks occurred at loading levels between 15-30 kN, which corresponds well with the tensile strengths of the concretes. The first (“unstable”) cracks appeared at short intervals along the specimen. By creation of each crack a sudden drop in load was observed. A stable phase ensued, and additional cracks were created. Just prior to the steel yielding the primary cracks have localized to 8 to 10 crack planes. The number of crack concords with the experimental results of Creazza et al. (1996), who used the same set-up and specimen dimensions as here, but the concrete prisms had a circular cross-section.

At deformations near yielding of the steel (at approximately 110 kN) splitting was detected at the ends of some elements. This occurred at load levels exceeding 90 kN and is explained by the Poisson’s effect which markedly diminishes the bonding. The cracks now grow in turn, as the yielding localizes in the steel and wanders along the rebar from one end to the other. This is reflected in a serrated curve where usually each drop represents the stage at which resistance of a crack surface is overcome. With increasing deformations the concrete body is almost segmented into separate blocks and longitudinal crack branches start to appear. This splitting phenomenon is also believed to be caused by the Poisson’s effect and slip.

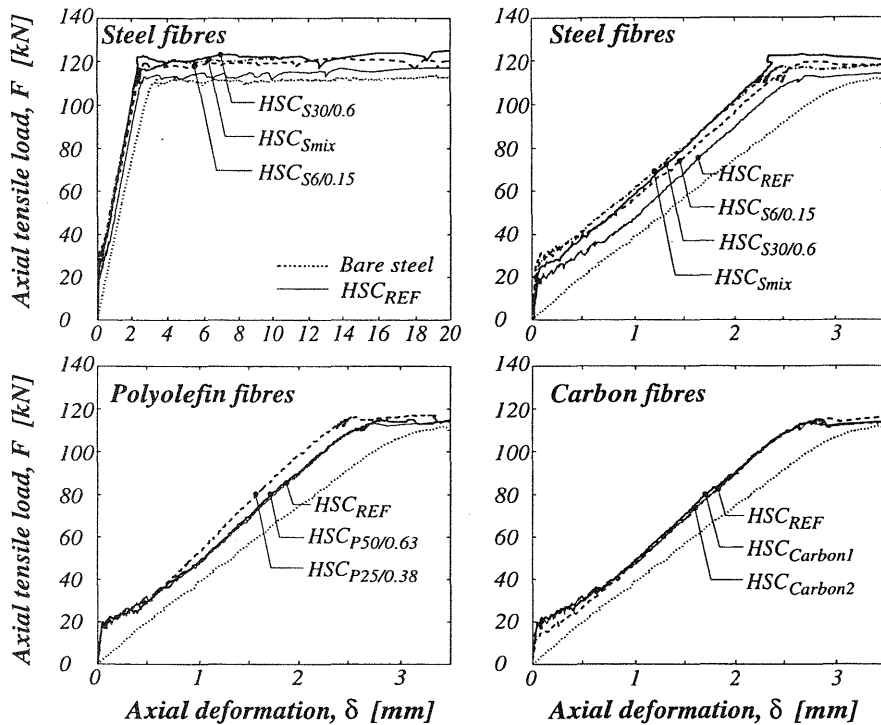


Fig. 3. The load-displacement responses of the tie elements.

4 Computational analysis by FEM - Inner softening band (ISB)

A preliminary finite element method (FEM) analysis was performed in Noghabai (1977a, c). The FE-model is based on an inner softening band (ISB) concept. A strong displacement discontinuity is inherent in the constitutive formulation of each element. It uses a plasticity type of model where the softening law is affined to the fictitious crack concept, hence CODs may be explicitly obtained, see Ohlsson and Olofsson (1997).

The analysis were performed at the time when material data from the experiments were not available. The FE-analysis here aim at understanding the underlying mechanisms and they should be compared with the experimental observations only in this sense. The results of the analysis are compiled in Fig. 4. Apart from a stress-strain relation for the steel rebar, the only input to the model is the E_c , f_{ct} , f_{cc} and σ_f -w relation. Since 1 volume-% fibres does not seem to influence much of either the E_c or the f_{ct} , the true variable in the analysis is the σ_f -w curves, see Fig. 1. Also the effect of a relative slip between the rebar and concrete has been studied.

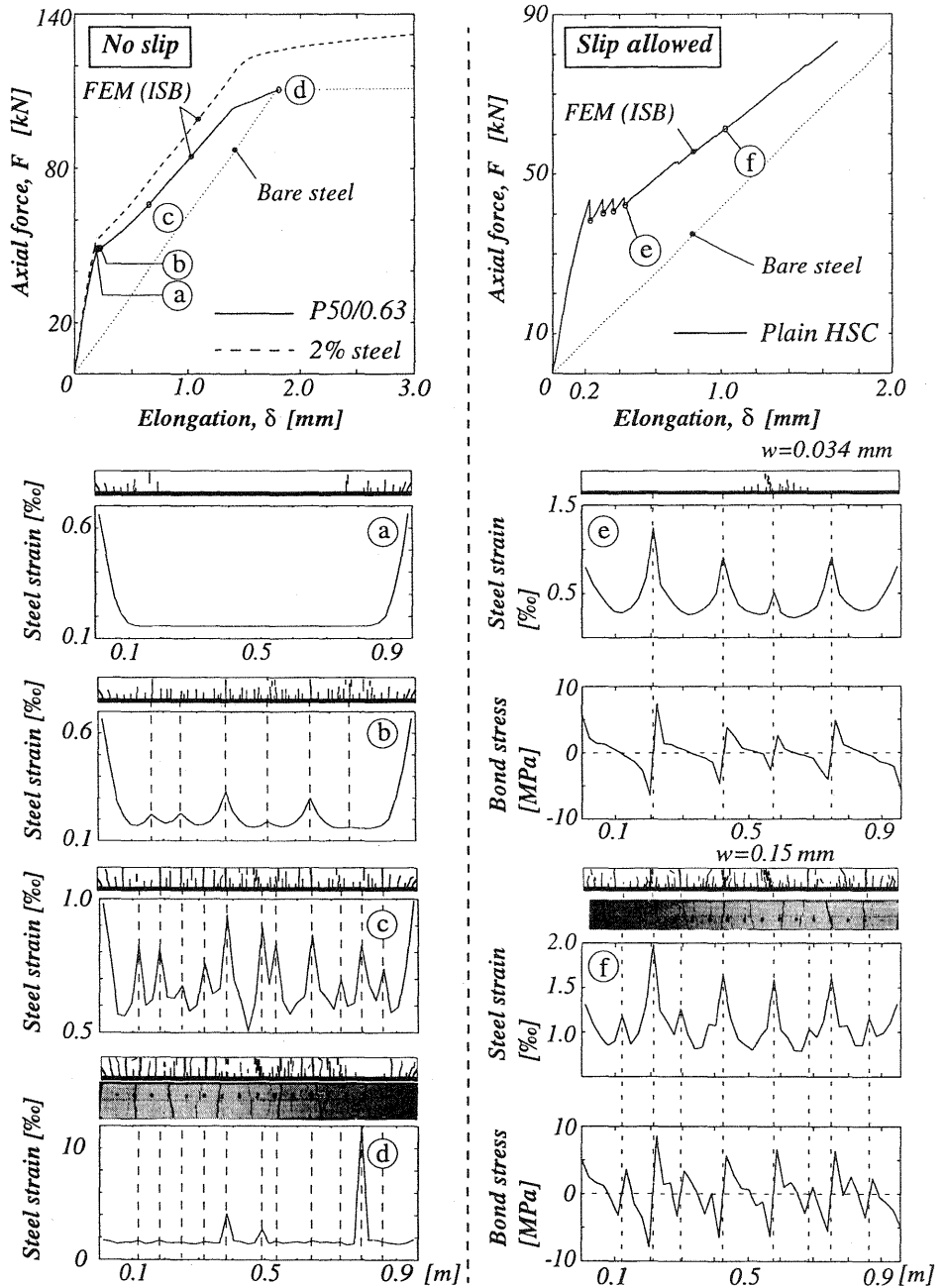


Fig. 4. FEM analysis by inner softening band (ISB) model, assuming perfect bond (left) and allowing a relative slip at the bar-to-concrete interface (right). Only the active softening bands (cracks) are displayed. Inlaid photos show cracked specimens.

In both cases, the mesh comprised 308 CST, plane-stress elements and 44 bar elements was used. The elements representing each material are given an equal quality. In the case of perfect bond the bar-elements connects the nodes of concrete-elements along the plane of symmetry. When slip is allowed, an interface layer (44 elements) with zero-thickness is modelled between the rebar- and concrete-elements. A local bond-relative slip ($\tau-\Delta$) relation according to CEB (1995) was assigned to the interface elements. The load is applied by a prescribed displacement of the node at the end of the bar. Iteration procedure was according to Newton-Raphson.

In Fig. 4 the force-elongation curves obtained by the ISB-model is given. The ISB patterns and some numerical values of calculated surface crack widths (w) are given, at the load levels indicated in the diagrams. For each given state, the obtained steel strains and their distribution along the rebar are presented, where each peak corresponds to a localized crack. In the case where slip is allowed also the distributions of the bond stresses are given. Both analysis indicate how a stable increase in the load becomes unstable at creation of primary cracks. This is reflected in the serrations in the $F-\delta$ diagram. The serrations become more conspicuous when a relative slip is allowed. It must be noted that the adopted $\tau-\Delta$ is based on a pull-out test of a rebar with short embedment length. Thus, the relation already incorporates the deformations associated with cracking in the surrounding concrete and consequently the total deformations obtained here have to be exaggerated. It is evident, not least against the background of the experiments, that the tension softening of concrete has a pronounced effect on the composite behaviour of rebars and concrete.

5 Analytical Model

The presented model is based on the cracking and the ensuing softening of the concrete and not on the assumption of a relative slip. The model can schematically be described as shown in Fig. 5a. Initially, both "springs" are activated and a superposition of their reaction forces balances the applied load, according to Eq. (1),

$$F = F_c + F_s = \sigma_c A_c + \sigma_s A_s \quad (1)$$

where σ_c , σ_s , A_c and A_s denote the stress and area of concrete and steel rebar respectively. By onset of softening in concrete Eq. (1) is allowed as long as a compatibility requirement for the system is met as given in Fig. 5a, thus $\delta = \delta_c = \delta_s$:

$$\delta = \left(\frac{\sigma_c}{E_c} + \frac{\bar{w}}{s} \right) L = \frac{\sigma_s}{E_s} L \quad (2)$$

where L is the length of the prism embedding the reinforcement, s is the average crack spacing, E_c and E_s are the moduli of elasticity for concrete and steel, and \bar{w} is the average crack opening. An incremental approach must be used to fulfil Eqs. (1) and (2) simultaneously, i.e. stepwise following the constitutive relations for the two components for a prescribed deformation.

In Fig. 5b the experimentally obtained F - δ curves are compared with the simulated ones for HSC_{REF} , $HSC_{S30/0.6}$ and $HSC_{S6/0.15}$. The results of the uniaxial tensile tests according to Fig. 3 have been implemented in Eqs. (1) and (2). According to Fig. 5b, the tension stiffening effect is clearly a function of the softening behaviour.

6 Conclusions

The influence of fibres on the tension stiffening effect is investigated by means of experiments as well as computational and analytical models. The models are based on the deformation softening of concrete in uniaxial tension. It is suspected that what has traditionally been attributed to a relative-slip in analytical models for tension stiffening effects, is largely due to the crack opening resistance (i.e. the softening behaviour) of concrete. It is believed that a possible slip occurs in conjunction with extensive cracking.

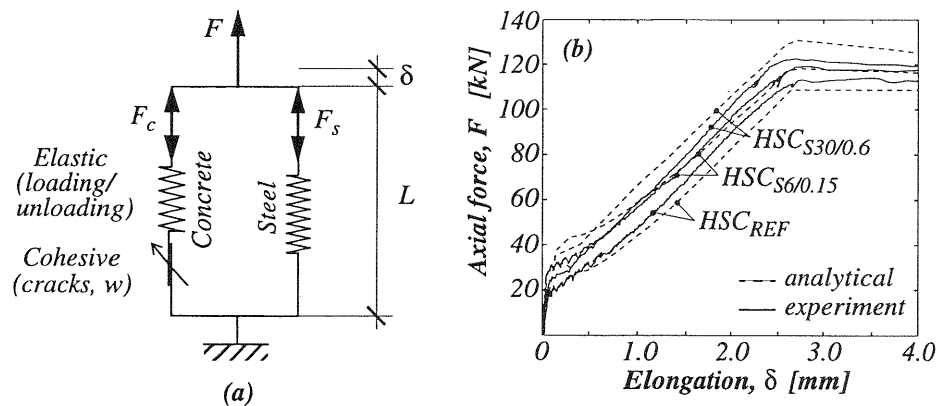


Fig. 5. a) The simple model describing a tie-element in tension. b) Comparison between the model predictions and the experiments. From Noghabai et al. (1997b).

7 Acknowledgement

The work was supported by the Swedish Council for Building Research (BFR) and the Swedish Research Council for Engineering Sciences (TFR). The research program was planned and conducted by Tech. lic. Noghabai, who also performed the FE-analysis. The analytical model was devised by Dr. Olofsson who supervised the work together with Prof. Dr. Elfgrén.

8 References

- CEB (1995) High Performance Concrete, Recommended Extensions to the Model Code 90, Research Needs, **Bulletin d'Information No 228**, Comité Euro-International du Béton (CEB), Stuttgart.
- Creazza G., Di Marco R., Russo S. and Siviero E. (1996) Tension stiffening in high strength concrete, in **Utilization of High-Strength/High-Performance Concrete** (eds. F. de Larrard and R. Lacroix), Paris, 1135-1143.
- Groth P. and Noghabai K. (1996) Fracture mechanics properties of steel fibre-reinforced high-performance concrete, in **Utilization of High-Strength/High-Performance Concrete** (eds. F. de Larrard and R. Lacroix), Paris, 747-756.
- Noghabai K. (1997a) Effect of various types of fibers on the bond capacity - Experimental, analytical and numerical investigations, in **ACI Spring Convention**, Seattle, (to be published).
- Noghabai K., Olofsson T. and Gustafsson J. (1997b) Fiber reinforced high-strength concrete beams in shear, in **First Engineering Foundation Conference on High-strength Concrete**, Hawaii, (to be published).
- Noghabai K. (1997c) Environmental effects on bond between deformed bars and concrete - A fracture mechanics approach, **CANMET/ACI International Conference on Durability of Concrete**, Sydney, 189-203.
- Ohlsson U. and Olofsson T. (1997) Mixed-Mode Fracture and Anchor Bolts in Concrete analysis with inner softening bands, **J. Engrg. Mech.**, 123(10), 1027-1033.
- RILEM TC 147-FMB (1996) Round Robin Analysis and Tests on Bond. **Materials and Structures**, RILEM, 29, Aug/Sept, 453-454.